Elastic Wave Modeling in Complex Geometries using Elastodynamic Finite Integration Technique

Prashanth Kumar CHINTA, Wolf KLEINERT

GE Sensing & Inspection Technologies GmbH; Huerth, Germany
Phone: +49 2233 601374; e-mail: prashanthkumar.chinta@ge.com, wolf.kleinert@ge.com

Abstract
This paper presents the results of a numerical computational tool "Elastodynamic Finite Integration Technique (EFIT)" for elastic wave modeling in complex geometries. The 2D-EFIT simulation results for complex geometries such as rail axles, rail tracks, rail wheels, and steel bars are presented. Depending on the application the simulations for contact and immersion techniques are performed. Various synthetic phased array transducers are modelled. Apart from the volumetric body waves i.e. pressure and shear waves, the surface waves and creeping waves are also investigated. These simulations were useful not only for the interpretation of ultrasonic echoes but provide us the valuable information regarding the transducer, with which a suitable transducer for a particular application is determined. The wave propagation results are presented in the format of movies and time domain snapshots to give better intuition in understanding scattering of elastodynamic waves.

Keywords: Ultrasonic Testing, Scattering, Numerical Modeling, EFIT, NDT.

1. Introduction

The elastodynamic wave propagation can be effectively simulated using numerical techniques. Although numerical modeling is relatively slow against semi-analytical methods they can be applied to real life NDT problems because of the advent of fast computers. The Finite Integration Technique (FIT) *[1]* is one helpful numerical method in solving the electromagnetic and elastodynamic wave field problems. Application of FIT to elastodynamics leads to the development of Elastodynamic Finite Integration Technique, popularly known in its abbreviated form as EFIT *[2, 3]*. In the past EFIT had proved very effective in modeling of transducers, wave scattering and mode conversion phenomenon in complex geometries *[4, 5, 6, 7, 8]*. It can also simulate the surface waves such as Rayleigh surface waves and creeping waves *[3]*. Here in this paper the results of EFIT modeling applied to complex geometries are presented. The influence of complexity in the geometry on elastic wave propagation can be identified with EFIT. In the Sec. 2 governing equations of EFIT have been presented. Section 3 contains different applications of 2D-EFIT.

2. Fundamental Equations of Elastodynamic Finite Integration Technique

The Elastodynamic Finite Integration Technique (EFIT) is a tool developed using the linear integral equations of elastodynamics: Newton-Cauchy's equation of motion (Eq. 1) and deformation rate equation (Eq. 2) *[3, 9]*. EFIT uses the dual orthogonal grid system and marching on in time algorithm *[2, 3]* where the velocity vector ($\underline{\mathbf{v}}(\underline{\mathbf{R}}, t)$) components and the elastic stress tensor ($\underline{\underline{\mathbf{T}}}(\underline{\mathbf{R}}, t)$) components are determined simultaneously using the leapfrog technique. For the simulations, the spatial and temporal discretization is performed sustaining the stability condition of EFIT. Material parameters volumetric mass density (ρ) and compliance tensor ($\underline{\underline{\underline{\underline{\mathbf{s}}}}}(\underline{\mathbf{R}})$) constitute for the determination of different elastic wave mode velocities in the material. In Eq. (1) and Eq. (2) the force density vector ($\underline{\mathbf{f}}(\underline{\mathbf{R}}, t)$) and the induced deformation rate tensor ($\underline{\underline{\mathbf{h}}}(\underline{\mathbf{R}}, t)$) respectively are the source terms.

$$\iiint_V \rho \frac{\partial}{\partial t} \underline{\mathbf{v}}(\underline{\mathbf{R}}, t)\, \mathrm{d}V = \oiint_{S=\partial V} \underline{\mathbf{n}} \cdot \underline{\underline{\mathbf{T}}}(\underline{\mathbf{R}}, t)\mathrm{d}S + \iiint_V \underline{\mathbf{f}}(\underline{\mathbf{R}}, t)\, \mathrm{d}V \qquad (1)$$

$$\iiint_V \underline{\underline{\underline{\mathbf{s}}}}(\underline{\mathbf{R}}) : \frac{\partial}{\partial t} \underline{\underline{\mathbf{T}}}(\underline{\mathbf{R}}, t)\, \mathrm{d}V = \oiint_{S=\partial V} \mathrm{Sym}\{\underline{\mathbf{n}}\, \underline{\mathbf{v}}(\underline{\mathbf{R}}, t)\}\, \mathrm{d}S + \iiint_V \underline{\underline{\mathbf{h}}}(\underline{\mathbf{R}}, t)\, \mathrm{d}V \qquad (2)$$

The indication "Sym" in Eq. 2 corresponds to the symmetrical tensor of $\underline{\mathbf{n}}\, \underline{\mathbf{v}}(\underline{\mathbf{R}}, t)$ where $\underline{\mathbf{n}}$ is the unit vector normal to the surface. The materials used for all the applications described in Sec. 3 are elastically isotropic materials.

3. Application of EFIT

Here in this section different applications of 2D-EFIT are presented.

3.1 Fundamental Simulation - Elastodynamic Wave Propagation and Scattering

In this section the simulation results of generation of creeping surface waves in steel (pressure wave velocity $\boldsymbol{c_P = 5940\, m/s}$, shear wave velocity $\boldsymbol{c_S = 3250\, m/s}$, and volumetric mass $\boldsymbol{\rho = 7840}$ kg/m^3 density) are presented. Besides observing surface waves we will study the wave scattering and mode conversion phenomena also. A normal incidence contact probe (transducer) with a centre frequency of 2MHz and a diameter of 15 mm is simulated. In the simulation all the boundaries are terminated with stress-free boundary condition. The wave propagation snapshots in time domain at different propagation times are presented in the Fig. 1. The Rayleigh surface waves which are generated during the excitation of the transducer propagate along the test specimen surface. They are indicated with "**R**". The head waves are indicated with "**H**". The incident pressure wave, indicated with "**P**", and a shear wave, indicated with "**S**" are diffracted by the cylindrical inhomogeneity. The resulting reflected pressure wave (indicated with **P→P**) and mode converted shear wave (indicated with **P→S**) are illustrated in Fig. 1. The cylindrical inhomogeneity also causes for the generation of creeping waves which are indicated with "**K**".

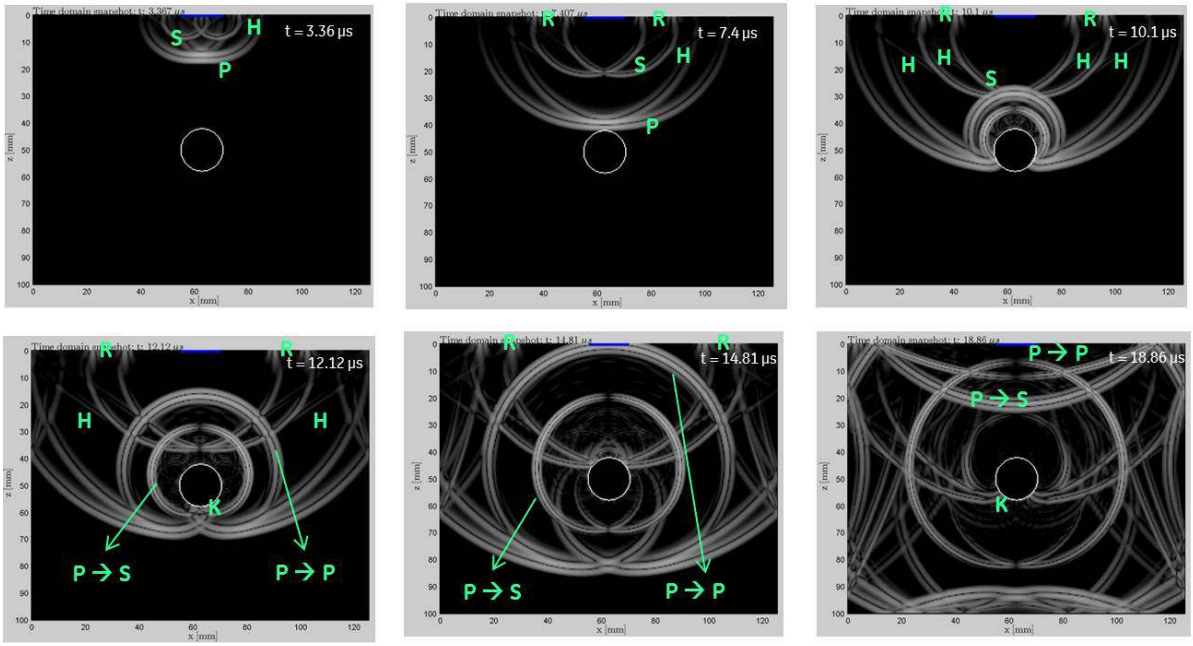

Figure 1. Elastodynamic wave propagation and scattering. Time domain snapshots of elastic wave propagation are displayed.

3.2 Defect Detection in Hexagonal Steel Bars

The hexagonal steel bars with a flat bottom hole (FBH) at the back wall and near to the corner have been simulated. An automatic testing machine ROWA by GE Inspection Technologies *[10]* has been developed to test such defects (notches and flat bottom holes) in steel bars of different shapes (cylindrical, rectangular, hexagonal, etc.) using immersion technique. The bars are introduced into a chamber where the pumped water is rotated continuously. The machine hosts the customized phased array transducers surrounding the bar. The number of phased array transducers depends on diameter of the bar, testing speed and defect (FBH) size. The virtual probes which are nothing but exciting some specified elements of the complete phased array probe are used to create a rotating ultrasound beam to cover the complete surface of the test specimen. Usually for cylindrical bars the transducers which impinge the longitudinal waves (pressure waves) with a normal incidence into the material are developed.

When testing hexagonal bars (see Fig. 2a) with FBH near to the corner, a weak signal from the tip of the FBH has been noticed. This is because of corners present at the transmission interface between water and steel. Hence to avoid the corner reflections and make use of the flat surface of the hexagonal bar a transducer that transmits shear waves into the bars making almost normal impact on the notch has been modeled using EFIT. Although the machine is based on immersion technique the simulation is performed by modeling an equivalent contact probe as the main motive is to check whether any defect signal can be observed from the tip of the FBH.

The transducer with a centre frequency of 5 MHz and with 10 mm projected shoe length on the bar has been modeled (see Fig. 2b). A Tukey aperture weighting is applied to supress the edge effects of the transducer. The shear wave has been introduced into the steel bar with an angle of 50°. The computational geometry (X × Z: 50 mm × 41 mm) has been discretized with grid cell size of 25 µm.

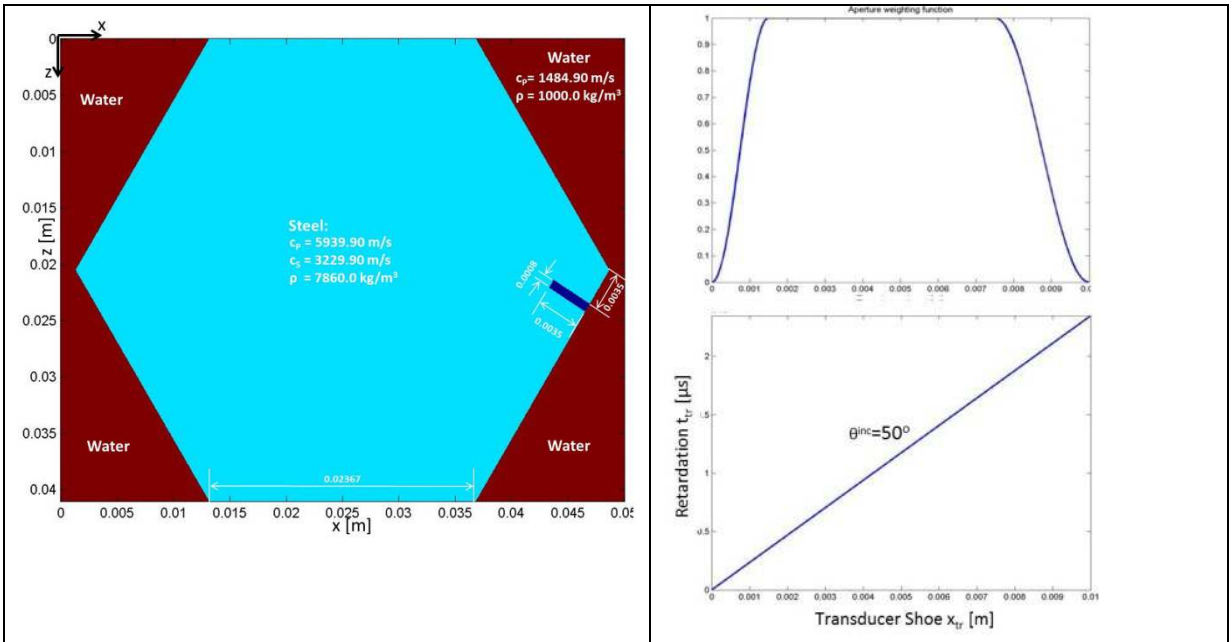

a) Geometry

b) Transducer modeling. Top: Amplitude weighting function. Bottom: Time retardation to achieve 50° shear wave incidence

Figure 2. Geometry and transducer modeling

The time domain snapshots of wave propagation resulted from 2D-EFIT simulation are displayed in Fig. 3. The incident shear wave is shown in Fig. 3a. Echo 1 is the mode converted pressure wave. Echo corresponds to the reflection of the shear wave by the notch. Echo 3 is the mode converted pressure wave reflected from the back wall. Echo 4 is the shear wave reflection from the back wall. Echo 2 is very clear and is the one required. This echo can be recorded by a receiver placed in the direction of echo marked as 6. Hence with such a transducer it is possible to obtain a good signal back from the FBH avoiding corner reflections.

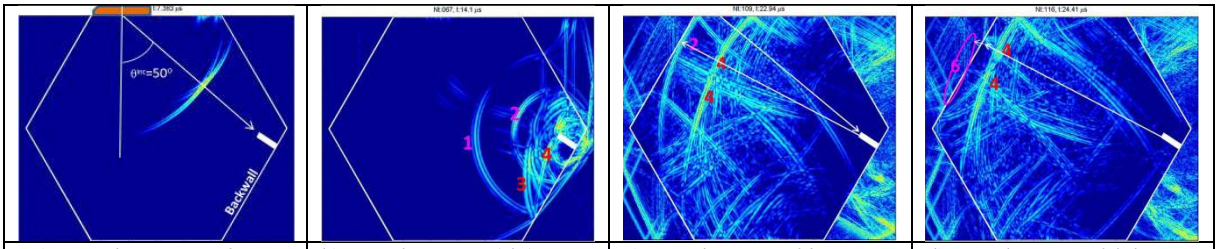

a) snapshot at t = 7.3 µs | b) snapshot at t = 14.1 µs | c) snapshot at t = 23 µs | d) snapshot at t = 24.4 µs

Figure 3. Time domain snapshots of elastodynamic wave propagation at different time instances.

3.3 Ultrasonic Testing of Rail Tracks

The detection of rail tracks has become important to ensure the safety of the passengers of a train. The NDT of tracks can be efficiently performed using ultrasonic testing. Here in this section 2D-EFIT simulation results for the detection of notch like defects (cracks) in the volume and at the surface are presented. To detect notches in the volume a transducer of normal incidence has been modeled. And the defects which protrude into the volume from the surface are modeld using sending and receiving phased array transducer pair. The Time-of-Flight Diffraction (TOFD) method has been exploited to determine the defect depth.

In Fig. 4 (left) the geometrical sections of the rail have been defined. A longitudinal wave transducer with 2MHz centre frequency and a shoe length of 15.6 mm has been modeled to detect the cracks in the vertical plane of the rail geometry. The normal incidence of longitudinal wave (pressure wave) on the crack results in a diffraction. The diffracted waves can be recorded by the same transducer. The diffractions of the elastic waves from the tip of the crack at different positions are illustrated in Fig. 5.

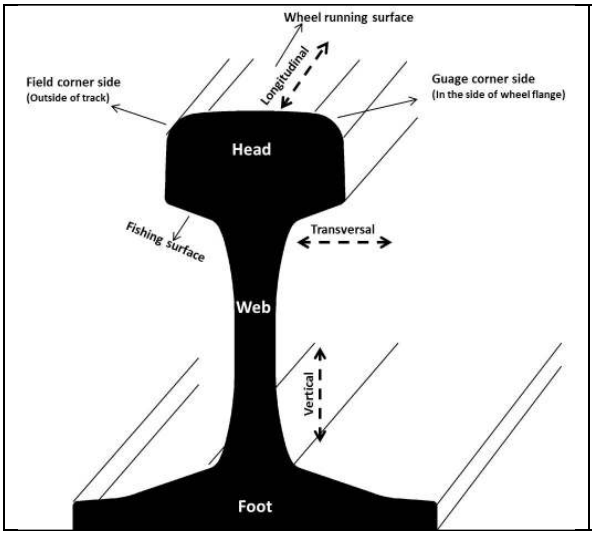

Material parameters:

c_P = 5940 m/s,

c_S = 3250 m/s, ρ=7860 kg/m^3

Transducer:

f_0 = 2 MHz, L = 15.6 mm.

Defect: notch

width: w = 1.5mm,

defect depth: d = 12 mm.

EFIT parameters:

dx = 100 µm,

(X × Z)= (150, 172) mm,

(Nx × Nz) = (1500, 1720) grid cells.

Figure 4. Left: Rail geometry. Right: Material parameters and EFIT discretization parameters

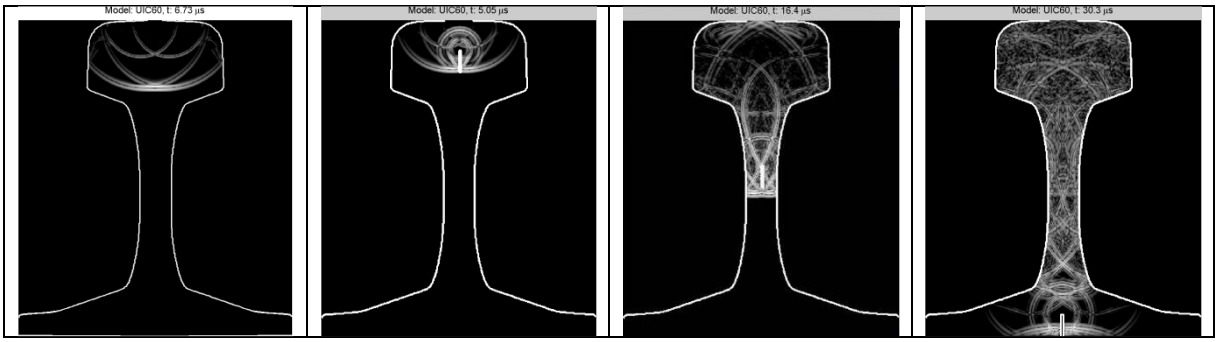

Figure 5. Time domain snapshots of elastodynamic wave propagation. a) Without defect – reference experiment. b) Diffraction when the notch is in the head part of the rail. c) Diffraction when the notch is in the web part of the rail. d) Diffraction when the notch is in the foot part of the rail.

The elastic wave diffraction from surface defects in the longitudinal plane (see Fig. 4) is also simulated using 2D-EFIT. A pair of phased array angle probes is modeled to detect the defects penetrating from the surface to the head part of the rail. The TOFD method is employed to determine the size of the defect. This model can work only when the depths of the defects are limited i.e. the depth should not exceed the depth of the head part of the rail. In this method the diffraction from the bottom tip of the defect will be recorded by the receiving transducer as illustrated in Fig. 6 and Fig. 7. Figure 6 corresponds to the simulation of the transducer with 60^o steering angle whereas Fig. 7 to the 70^o steering angle. Both wave modes i.e., diffracted pressure wave and shear wave can be used to determine the depth. These diffracted wave modes are indicated with "**P**" and "**S**" in Fig. 6 and Fig. 7. The sending and receiving transducers are also marked with thick red and blue lines respectively. Since the offset between the transducers (x) and incidence angle are known the depth of the defect can be easily calculated. If s is the sound path distance and θ is the steering angle then the depth (d) of the defect is computed using $d = s\,cos(\theta)$.

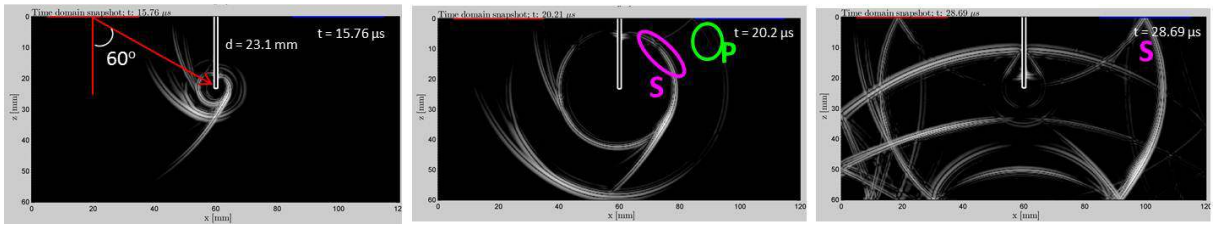

Figure 6. TOFD using 60^o shear wave angle probe. The defect depth is 23.1 mm

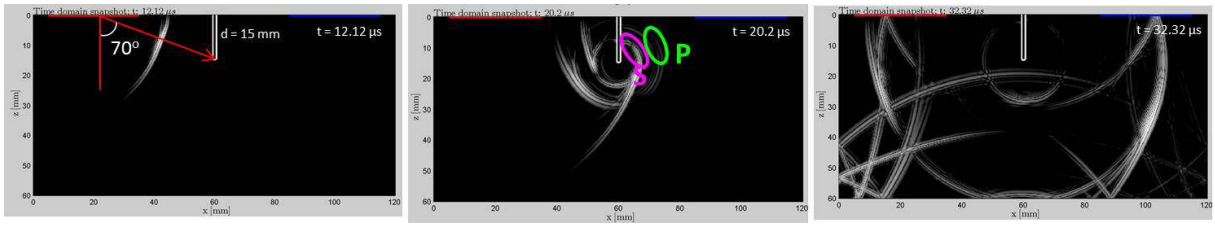

Figure 7. TOFD using 70^o shear wave angle probe. The defect depth is 15 mm.

3.4 2D-EFIT Simulations for Rail Wheel Set Testing

The detection of defects on the web surface of the wheel of a train is a challenging task because of its complex geometry. Sometimes the defects are shadowed because of the holes present in the wheel geometry. For transversal defects (defects oriented perpendicular to the radial line) V-transmission method is applied (see Fig. 8).

For 2D-EFIT simulations an ICE3 train wheel from Deutsche Bahn, Germany has been used. The geometry of the part of a wheel is shown in the Fig. 8. The diameter of the probe mounting surface is 920 mm. A sending and receiving phased array transducers are arranged with an offset of 250 mm. These transducers work in V-transmission method. The aim of the simulation is to determine the suitable incidence wave mode to detect the defects at larger depths. The geometry, probe arrangement and defect position used for the simulation are shown in Fig. 8. A pressure wave and shear wave transducers with a steering of 17^{o} and a centre frequency of 2 MHz are modeled. The projected shoe length of the transducer is 30 mm. The geometry of size 550 mm × 460 mm is discretized into 5500 × 4600 grid cells with a grid cell size of 100 µm. For the simulations all the boundaries of the geometry are terminated with stress-free boundary condition. The aim of the simulation is to check which transducer is useful for such defects.

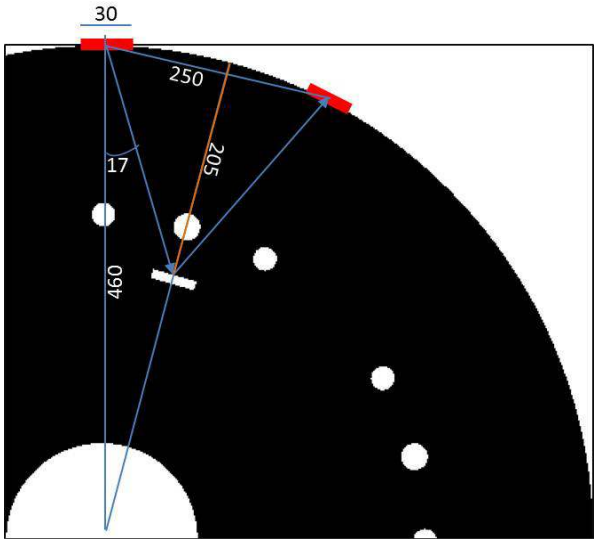

Figure 8. Part of ICE 3 wheel geometry. The transducer arrangement for V-transmission is also depicted.

The results of the 2D-EFIT simulation with pressure wave transducer are illustrated in Fig. 9. The pressure wave makes an impact with defect at an incident angle of 17^{o}. The reflected pressure wave from the defect, marked as echo 3, is recorded by the receiver. The A-scan obtained is depicted in Fig. 10. The results of the similar experiment with shear wave transducer are presented in Fig. 11. The corresponding A-scan is shown in Fig. 12. The echo 3 is the defect echo. The A-scans are normalized to pulse amplitude when the incidence is normal. Echoes 1 is because of edge effect of the transducer and echo 2 is the reflection from the hole in the geometry. From the comparison it is clear at lower angles ($<30^{o}$) pressure wave probe are preferred.

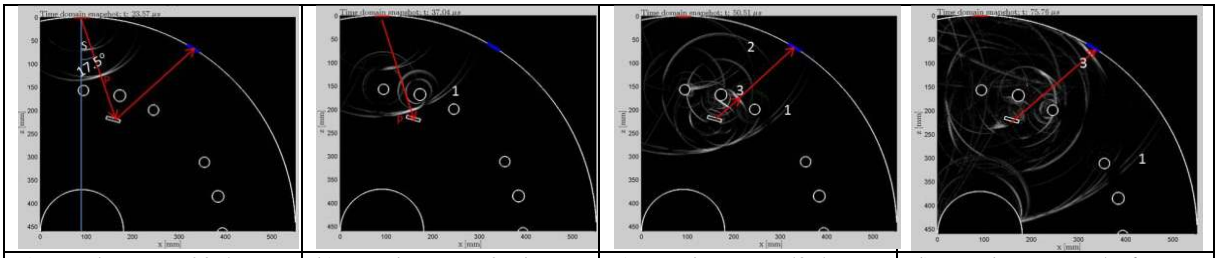

a) snapshot at t = 23.57 µs	b) snapshot at t = 37.4 µs	c) snapshot at t = 50.5 µs	d) snapshot at t = 75.76 µs

Figure 9. Time domain snapshots of elastodynamic wave propagation at different times. Echo 3 is the defect echo. Echo 1 is due to the edge effect of the transducer. Echo 2 is due to the reflection from the hole.

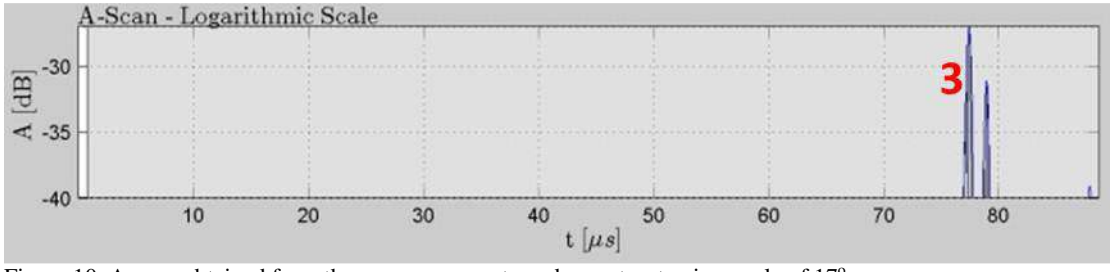

Figure 10. A-scan obtained from the pressure wave transducer at a steering angle of 17°.

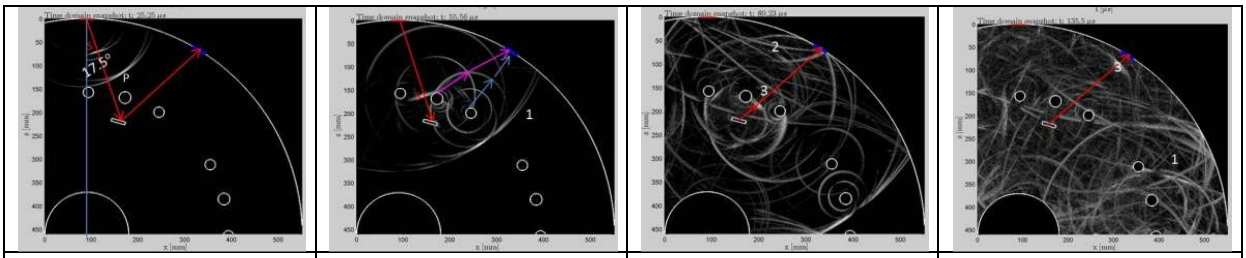

a) snapshot at t = 23.57 μs	b) snapshot at t = 37.4 μs	c) snapshot at t = 50.5 μs	d) snapshot at t = 75.76 μs

Figure 11. Time domain snapshots of elastodynamic wave propagation at different times. Echo 3 is the defect echo. Echo 1 is due to the edge effect of the transducer. Echo 2 is due to the reflection from the hole.

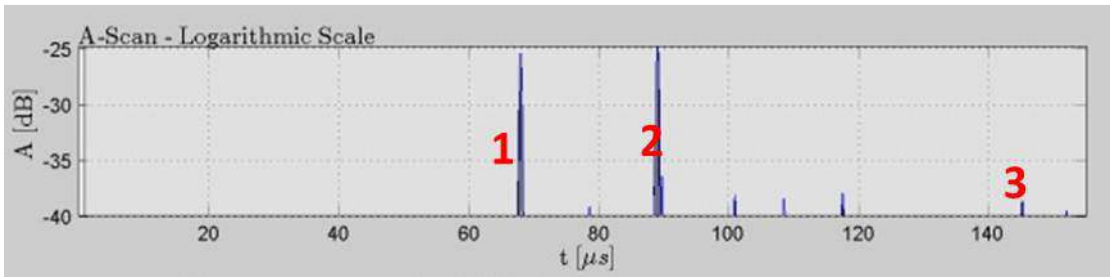

Figure 12. A-scan obtained from the shear wave transducer at a steering angle of 17°.

4. Conclusions

In Sec. 3.1 the generation creeping waves of the cylindrical inhomogeneity is simulated with EFIT. The generation of creeping wave depends on the radius of the cylindrical inhomogeneity and frequency of transducer beam. In Sec. 3.2 the transducer has been modeled to detect the FBH near to the corners of a hexagonal steel bars. The TOFD and diffraction of elastodynamic waves are investigated and presented in Sec 3.3. The defect depths have been estimated using TOFD method. EFIT has successfully simulated the V-transmission model and was able to determine the preferred transducer at lower steering angles. It has been found from the results presented in Sec. 3.4 that at lower angles pressure wave transducers are preferred over shear wave transducers.

References

1. Weiland, T.: Eine Methode zur L¨osung der Maxwellschen Gleichungen f¨ur sechskomponentige Felder auf diskreter Basis. AE¨ U, Bd. 31, Vol 3, pp. 116-120, 1977.
2. Fellinger, P., Marklein, R., Langenberg, K. J., Klaholz, S.: Numerical modeling of elastic wave propagation and scattering with EFIT - elastodynamic finite technique. Wave Motion, Vol. 21, pp. 47-66, 1995.

3. Marklein, R.: Numerische Verfahren zur Modellierung von akustischen, elektromagnetischen, elastischen und piezoelektrischen Wellenausbreitungsproblem im Zeitbereich basierend auf der Finiten Integrationstechnik. Dissertation: University of Kassel, Germany, 1997.
4. Marklein, R., Langenberg, K. J., Mayer, K.: EFIT Simulations for Ultrasonic NDE. In: Proceedings of the 8th European Conference for NonDestructive Testing (ECNDT), Barcelona, Spain, June 17-21, 2002.
5. Marklein, R., Chinta, P. K., Langenberg, K. J., Hintze, H., Plankert, W.: Numerical Modelling of Ultrasonic NDT of a Wheel Shaft of an ICE Train, In: Proceedings of the 9th European Conference for NonDestructive Testing (ECNDT), Berlin, Germany, 2006.
6. Chinta, P. K., Mayer, K., Langenberg, K. J.: Numerical Modeling of Elastic Inhomogeneous Anisotropic Media Using 3D-Elastodynamic Finite Integration Technique. AIP Conference Proceedings: Vol. 1433, International Congress of Ultrasonics (ICU), Gdansk, Poland, 2011.
7. Chinta, P. K., Mayer, K., Langenberg., K. J., De Odorico, W., Koch, R., Maurer, A.: Numerical Modelling of Ultrasonic Phased Array Transducers and their Application, In: Proceedings of the 9th European Conference for NonDestructive Testing (ECNDT). Berlin, Germany, 2006.
8. Chinta, P., Mayer, K., Langenberg, K. J., Prager, J.: Three-Dimensional Elastic Wave Modeling in Austenitic Steel Welds using Elastodynamic Finite Integration Technique, In: Proceedings of 18th World Conference on Nondestructive Testing, Durban, South Africa, 16-20 April 2012.
9. Langenberg, K. J., R. Marklein, K. Mayer: Ultrasonic Nondestructive Testing of Materials: Theoretical Foundations. CRC Press, Boca Raton, 2012.
10. ROWA - Tube/Pipe Tester: http://www.ge-mcs.com/en/ultrasound/integrated-systems/bar-rowa.html.